

# PHOTONICS Research

## Low-threshold and narrow-emission random lasing in a self-assembly TiN nanoparticle-doped carbon quantum dot/DCM nanowire composite

JING LYU,<sup>1,2</sup> XINYU ZHANG,<sup>1</sup> LEI CAI,<sup>3</sup> LI TAO,<sup>1,4</sup> WEIFENG MA,<sup>1</sup>  AN LI,<sup>1</sup> YE TIAN,<sup>1</sup> YUNSONG YIN,<sup>1</sup> DENAN KONG,<sup>1</sup> WEN YI,<sup>1</sup> XIANSHUANG WANG,<sup>1</sup>  AND RUBIN LIU<sup>1,\*</sup>

<sup>1</sup>Beijing Key Laboratory of Nano-photonics and Ultrafine Optoelectronic Systems, School of Physics, Beijing Institute of Technology, Beijing 100081, China

<sup>2</sup>Yangtze Delta Region Academy of Beijing Institute of Technology, Jiaxing 314000, China

<sup>3</sup>Jiangsu Key Laboratory for Carbon-Based Functional Materials & Devices, Institute of Functional Nano & Soft Materials (FUNSOM), Soochow University, Suzhou 215123, China

<sup>4</sup>e-mail: litao@bit.edu.cn

\*Corresponding author: liusir@bit.edu.cn

Received 3 May 2022; revised 23 July 2022; accepted 24 July 2022; posted 26 July 2022 (Doc. ID 462588); published 1 September 2022

The random lasing in quantum dot systems is in anticipation for widespread applications in biomedical therapy and image recognition, especially in random laser devices with high brightness and high monochromaticity. Herein, low-threshold, narrowband emission, and stable random lasing is realized in carbon quantum dot (CQD)/DCM nanowire composite-doped TiN nanoparticles, which are fabricated by the mixture of carbon quantum dots and self-assembly DCM dye molecules. The Förster resonance energy transfer process results in a high luminescence efficiency for the composite of carbon dots and DCM nanowires, allowing significant random lasing actions to emerge in CQD/DCM composite as TiN particles are doped that greatly enhance the emission efficiency through the plasmon resonance and random scattering. Thus, sharp and low-threshold random lasing is finally realized and even strong single-mode lasing occurs under higher pumping energy in the TiN-doped CQD/DCM composite. This work provides a promising way in high monochromaticity random laser applications. © 2022 Chinese Laser Press

<https://doi.org/10.1364/PRJ.462588>

### 1. INTRODUCTION

Random lasers have attracted great interest in the scientific community for their simple structure, easy fabrication, low cost, and low spatial coherence properties [1–4]. However, the development of random lasers is restricted by the poor controllability, high energy loss, and complex modes owing to the randomness of multiple scattering. The quantum dots with narrow bandwidth emission and high fluorescence efficiency can deal with these problems and contribute to the development of ultra-stable and low-threshold random lasers with high brightness and high monochromaticity [5–7]. Hence, the random lasing in quantum dots is in anticipation for widespread applications from military weapons, biomedical therapy, image recognition, and especially in nano random laser devices [8–12]. In particular, carbon quantum dots (CQDs), which were first obtained by Xu group in 2004, show great promise with strong fluorescence. In addition, CQDs are regarded as superior to conventional semiconductor quantum dots due to a number of excellent properties such as water solubility, low cost, chemical inertness, high stability, low toxicity, and

biocompatibility, which indicates that CQDs can be a good choice for laser gain materials and nanophotonic light sources [13–20]. It is possible to use CQDs as a gain media for random lasers. The random lasers based on pure quantum dot systems have been developed to date. However, the random laser efficiency and intensity are low. One possible reason is the low optical gain generated by quantum dots. Another one is that the quantum dots typically have sizes of ~10 nm, which cannot trigger the scattering feedback mechanism in random lasing, since efficient scattering requires structure sizes which are comparable to the pump light wavelength. Researchers have improved the gain efficiency and scattering of the quantum dot system by means of fabricating a composite structure or doping materials [21–25].

In the past 5 years, many types of carbon quantum dot lasers have been experimentally demonstrated and many applications have been proposed in optical devices. In 2016, Jiang's group found random lasing behavior in surface functionalized carbon quantum dots/RhB composite [15]. Then Liao and Lin's group also observed the efficient and tunable random laser

in carbon-dot-decorated nanostructured semiconductors in 2018 [18]. In this work, we discover the random lasing action in CQD/DCM nanowire composite doped with TiN nanoparticles (C/D/T), which are fabricated by the DCM dye molecules self-assembly. The fluorescence efficiency of CQD/DCM nanowire composite is enhanced compared to pure DCM due to the Förster resonance energy transfer (FRET) process [14,15]. In addition, the TiN particles are doped in composite as the enhancement media of plasmon resonance and scattering. Due to the contribution above, we find the low-threshold, narrowband emission, and stable random lasing in C/D/T composite. More specifically, the ultra-sharp random peaks behave as approximately strong single-mode lasing, which has prospect in application to high brightness and high monochromaticity random laser [14,20,26]. It can be found that many CQDs adhere on the surface of self-assembly DCM nanowires and the irregular nanowires also enhance the random scattering, which contributes to the lasing actions of the C/D/T composite system. The random lasing is also enhanced by plasmon resonance and scattering from TiN [27–36].

## 2. EXPERIMENTAL SECTION

### A. Preparation of Sample Solutions

(1) DCM nanowire solution: We dissolved the DCM dye into dimethyl sulfoxide (DMSO) solution for 40-min ultrasonic vibration and the concentration of solution is 0.7% (mass fraction). Then we let the DCM dye solution stand still for 12 h. The DCM dye molecules self-assembled into DCM nanowires in solution. (2) CQD/DCM composite solution: The CQD solution was mixed with the DCM dye nanowire solution with the weight ratio of 1:1 and the concentration of DCM nanowire solution is 0.7% (mass fraction). The mixture solution was put into an ultrasonic machine in beaker for 20-min ultrasonic vibration. The mixture solution stood still for 1 h. Then we got the CQD/DCM composite solution. (3) CQD/DCM composite-doped TiN nanoparticle (C/D/T) solution: We dissolved TiN particles (the diameter is 40 nm) in the CQD/DCM mixed solution for 40-min ultrasonic vibration and the sample solution stood still for 1 h. The weight ratio of

the CQD/DCM solution and TiN solution is 5:1 and the concentration of TiN is 1 mg/mL.

### B. Measurement

The absorption spectrum and emission spectrum of DCM dye molecules and carbon quantum dots were recorded by a UV-Vis spectrophotometer. For investigating the lasing actions in CQD/DCM composite-doped TiN nanoparticles, each sample solution is injected into a quartz capillary with the diameter of 300  $\mu\text{m}$  and length of 200 mm. The sample capillaries are excited by the Nd:YAG pulse laser (532 nm, 10 ns pulse, 10 Hz). Emission spectra of the sample were collected by the fiber spectrometer (AvaSpec-2048, 470–690 nm, 0.04–20 nm). The time-resolved photoluminescence (PL) spectra of CQD, CQD/DCM, and DCM were recorded by a time-correlated single-photon counter (PMA182-N-M), and the Fourier transform infrared spectroscopy (FTIR) spectra of pure DMSO solution, DCM solution, and CQD solution were collected by FTIR spectrometer (Thermo-IS5). All experiments were observed at room temperature.

## 3. RESULTS AND DISCUSSION

As shown in Fig. 1(a), the absorption spectrum of CQD and the emission spectrum of DCM are overlapped in the wavelength range of 540–650 nm, which is essential for the FRET process [15]. The center of the CQD absorption spectrum is 570 nm and the center of the DCM emission is 645 nm. Figure 1(b) shows that the emission spectrum image of CQD and the center of wavelength is 673 nm. The diameters of CQDs are around  $\sim 6$  nm, as shown in the inset SEM image. The DCM dye molecules act as donors and transfer energy to the CQD, which is the recipient in the FRET process. Moreover, the emission spectrum in Fig. 1(a) is from the DCM dye, which is DMSO solution and the concentration is 0.1% (mass fraction). The molecules have not self-assembled into nanowires when the concentration is 0.1% (mass fraction). The DCM dye solution does not show appreciable optical effects of micro-cavity and scattering, which is evidenced by the broad emission spectrum of DCM in Fig. 1(a). Furthermore, DCM with a concentration of 0.7% (mass fraction) is the

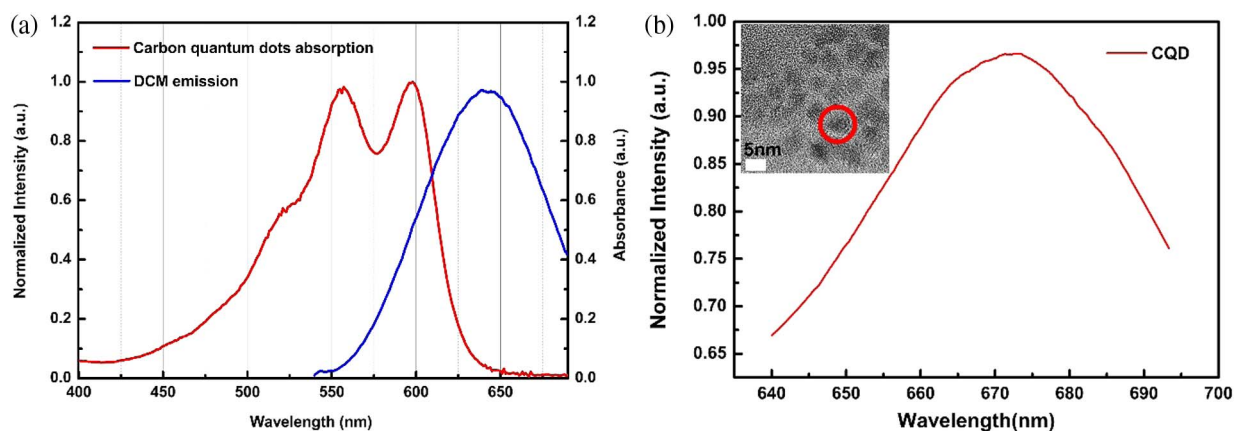


**Fig. 1.** (a) The absorption spectrum of carbon quantum dots and emission spectrum of DCM dye solution. (b) Emission spectrum of carbon quantum dots and an SEM image of carbon quantum dots.

primary material in fabricating the CQD/DCM composite structures because the DCM dye molecules can well self-assemble into nanowires under that concentration [33,34,37].

Figure 2 shows the home-built experimental setup for PL spectrum acquisition. The pump light is the nanosecond pulse laser (10 ns, 10 Hz, and 532 nm). The beam is split into two parts. One part is the referent light for energy detection. The other beam passes through the cylindrical lens along the horizontal optical axis and converges into a narrow line. The focal line irradiates on the sample and the emission spectra of sample are collected by the fiber spectrometer (Avantes, 470–690 nm).

The insets at the upper left are the optical micro-images of the capillary filled with the sample mixture. The mixture solution was injected into the capillary, which is 300  $\mu\text{m}$  in diameter, by a pipettor. We prepared three kinds of mixture solutions and injected them into capillary tubes. The three sample solutions are as follows: (1) self-assembled DCM dye nanowires solutions, (2) CQD/DCM solutions mixed with carbon quantum dots and DCM nanowires, and (3) CQD/DCM solutions doped with TiN nanoparticles (C/D/T); the solutions are mixed by CQD/DCM composites and TiN nanoparticles.

We prepared the DCM nanowires sample by the DCM dye solution with the concentration of 0.7%. Figure 3(a) shows the SEM image of DCM dye nanowires. The inset at the upper left shows the molecular structure of DCM dye. The inset at the upper right is the enlarged SEM image of the part marked by the red circle. From the SEM image of the DCM dye, we observed that the diameter of the self-assembled DCM nanowires with the concentration of 0.7% is around 4.15  $\mu\text{m}$ . Because of the planar aromatic ring structure of DCM dye molecules, the  $\pi - \pi$  stacking in molecules allows the dye molecules to self-assemble and crystallize into large-size nanowires in the sample solution with high concentration [15,31,34].

To investigate the energy transfer in the CQD/DCM composite, we analyzed the emission spectrum of DCM dye nanowires. Figure 3(b) presents the emission spectra of DCM

nanowire solutions in the capillary tube under different pump energies, showing center wavelengths at  $\sim 643$  nm. As the energy of the pump laser pulse increases, several small peaks emerge around the emission center, indicating the random scattering in the nanowires. The random lasing is absent in DCM nanowires due to the few effective oscillating routes and the FWHM of DCM nanowires in the tube is broad, as shown in Fig. 3(c). With the pump energy increasing from 65.8 to 205  $\mu\text{J}/\text{pulse}$ , the FWHM decreases from 22.4 to 20.1 nm. On account of the broad FWHM, the emission in DCM nanowires is just the spontaneous photoluminescence.

The CQD/DCM composite solution was injected into a capillary tube and excited by a nanosecond pulsed laser. Figure 3(d) shows the SEM image of the CQD/DCM composite and the distribution image of the carbon element corresponding to the region in the red dashed circle. It can be observed that the DCM dye molecules have self-assembled to dendritic nanowires. The DCM nanowires are surrounded by some aggregates of particles, which can be clearly seen in the region marked by the red dashed circle. The aggregates are CQDs, which can be confirmed by the carbon element distribution in the inset of Fig. 3(d). The DCM dye molecules form a large number of irregular nanowire structures by self-assembly and the CQDs mixed in the solution possess the hexagon molecular structure with  $\text{sp}^2$  hybrid [31,38,39]. The CQD/DCM composite structure is formed by van der Waals interaction and the CQDs are attached on the surface of the DCM nanowires [40]. Hence, the CQD/DCM composite can meet the distance requirement of FRET: the distance between donor and recipient is less than 10 nm.

Figures 3(e) and 3(f) show the emission spectra and FWHM of the corresponding emission spectrum as a function of the pump energy for the CQD/DCM composite in the capillary tube. As shown in Fig. 3(e), the small peaks emerge at the pump energy of 190.6  $\mu\text{J}/\text{pulse}$ . It indicates that the random lasing occurs in the CQD/DCM nanowire composite solution.

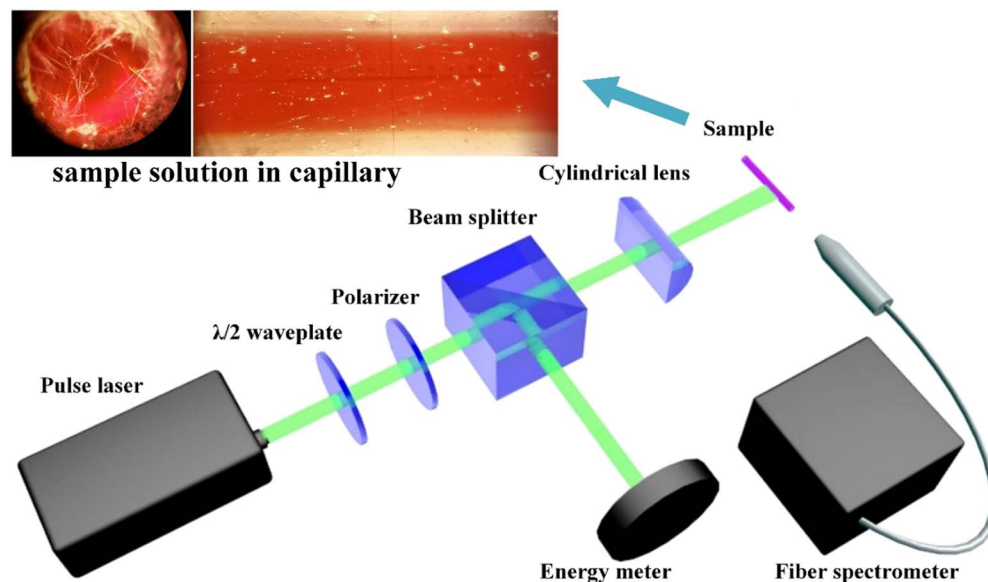
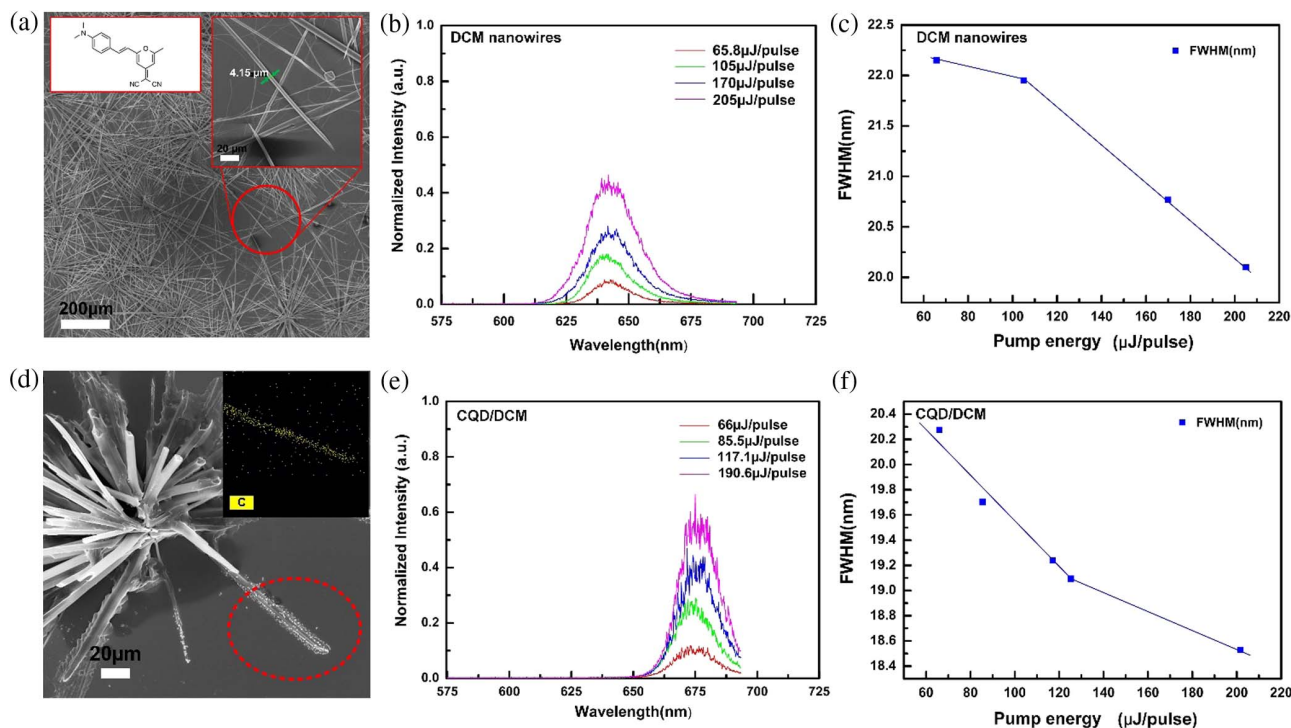


Fig. 2. Experiment setup for PL spectrum collection of composite solution.



**Fig. 3.** (a) The SEM image of DCM dye with the concentration of 0.7% (mass fraction). (b) The emission spectra of DCM nanowires solution in a capillary tube. (c) The full width at half-maximum (FWHM) of emission spectra of DCM nanowires solution in a capillary tube as a function of the pump energy. (d) The SEM image of CQD/DCM composite and the distribution image of carbon element corresponding to the SEM image of CQD/DCM composite inside the red dashed circle. (e) The emission spectra of CQD/DCM solution in a capillary tube. (f) The FWHM of emission spectra of CQD/DCM composite solution in a capillary tube as a function of the pump energy.

In comparison with the DCM nanowires, the emission of CQD/DCM composites shows narrower emission and higher intensity, which demonstrates that the efficient FRET process occurs in CQD/DCM solution. The donor DCM dye can transfer the energy into the acceptor CQD by the interface interaction, leading to a higher emission efficiency of the CQD. In addition, the emission center (680 nm) of CQD/DCM generates a redshift compared to the center of DCM (643 nm). The emission center of the CQD/DCM composite is close to that of the CQD (673 nm), which further confirms the FRET in the DCM and CQD [14,15].

More specifically, Figs. 3(b), 3(e) and 3(c), 3(f) show that the emission spectrum width and FWHM of CQD/DCM composites are significantly narrower than that of DCM nanowires correspondingly. Due to the amplified spontaneous emission, the spectra narrow gradually with the pump energy increasing. In Figs. 3(c) and 3(f), the FWHM of the CQD/DCM composites is narrower than that of the DCM nanowires under the same pump energy. The reason for narrower FWHM of CQD/DCM is the energy transfer. The DCM dye nanowires absorbed the pump energy and then transferred it to the CQD, which allows more photons to radiate from the center emission wavelength of the CQD. Therefore, the composite structure promotes the ultra-narrow emission from the CQD, and the narrow bandwidth emission is beneficial to the formation of sharp random lasing peaks in C/D/T solution.

To enhance the emission of CQD/DCM nanowire composite, we dissolved TiN particles in the CQD/DCM

mixed solution to prepare the C/D/T solution. Due to the presence of TiN particles, both plasmon and scattering are enhanced in C/D/T solution. As shown in Fig. 4(a), the sharp peaks appear in the spectrum of C/D/T solution in the capillary tube. The laser peaks appear and gradually rise with the increase of pumping energy. The center wavelength of the emission is 680 nm, and the emission width (10 nm) is further narrower compared to the emission width of the CQD/DCM composite without TiN particles. The lasing threshold of C/D/T solution is 356  $\mu\text{J}/\text{pulse}$ , as shown Fig. 4(b). The FWHM of the emission spectrum has already been within 10 nm before the lasing peaks appear. When the pump energy reaches 472  $\mu\text{J}/\text{pulse}$ , the sharp peaks emerge at the wavelength of 680 nm and the FWHM is only 0.29 nm. When the FWHM of peaks is within 1 nm, the coherent random lasing appears in the C/D/T composite solution. Photons can return to their original positions with scattering and form a ring cavity, which results in coherence lasing.

More interestingly, the laser peaks emerge as single-mode lasing with high signal-to-background ratio in Fig. 4(a), which is different from the conventional random laser [41]. The inset of Fig. 4(a) is the enlarged random lasing spectrum with the 472  $\mu\text{J}/\text{pulse}$  pump energy. We zoom in the figure with a range of 660–690 nm for the detailed lasing peaks. And we fit the spectrum curve with Gauss function. So we can identify the single lasing peak. According to the fitted curve, the photoluminescence emission is a broad Gauss curve. The enlarged spectrum shows a high and sharp lasing peak in the

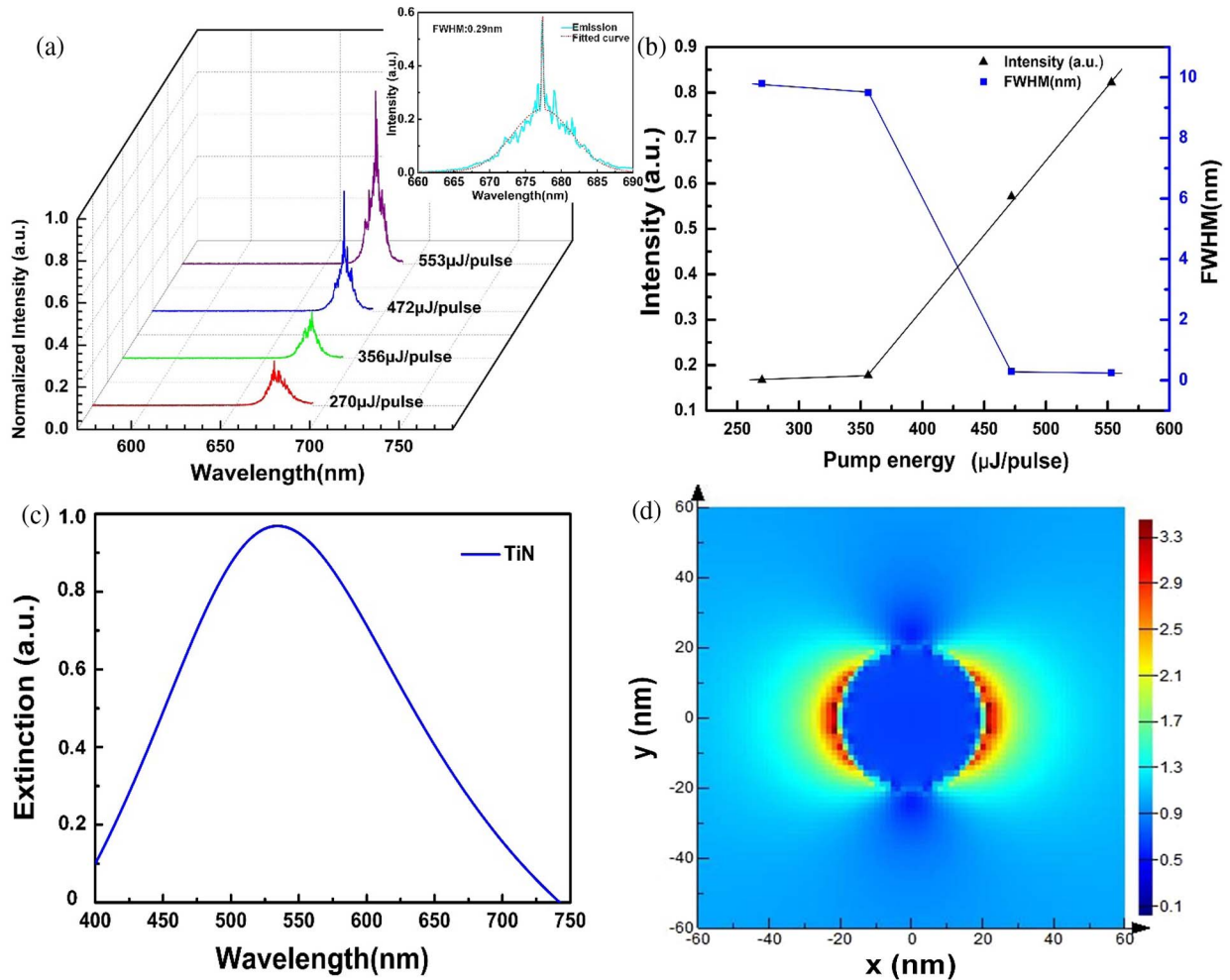


**Fig. 4.** (a) The random lasing emission spectra of CQD/DCM-doped TiN nanoparticles (C/D/T) solution in a capillary tube. (b) The peak intensity and FWHM of emission spectra of C/D/T solution in a capillary tube as a function of the pump energy. (c) The normalized extinction section of TiN nanoparticles with diameters of 40 nm. (d) The electric field intensity distributions around TiN nanoparticles with diameters of 40 nm at the wavelength of 680 nm.

photoluminescence emission center and the peak intensity is more than twice as high as the photoluminescence emission fitted. Several small peaks are near the emission center while their intensity is lower compared with the central strong peak. Therefore, when the central lasing peak is much higher than other peaks, we conclude that it can be approximated as single-mode lasing.

The reason for single-mode lasing is that narrow bandwidth emission and energy transfer of the CQD/DCM composite enable more amplified stimulated emission to emerge at the center wavelength, which means the oscillating route formed by random scattering is stable and high-quality to allow many times optical oscillating. On the other hand, the gain will reduce rapidly at other wavelengths due to the competition of gain. When the pump energy is beyond the threshold, there are a few amplified laser modes near the center wavelength and they absorb the energy of other peaks during the competition process of lasing, and thus a single-mode laser emerges. Note that the lasing behavior is generated only after the TiN particles doping, suggesting that plasmon enhancement and random scattering

between particles play vital roles in the lasing phenomenon of C/D/T solution [42].

In order to directly explain the efficient effect of TiN in the lasing behavior of the C/D/T composite, we simulated the extinction section of the TiN nanoparticles and electric field intensity distributions around the TiN nanoparticles by the finite-difference time-domain method. As shown in Figs. 4(c) and 4(d), the extinction spectrum indicates that the TiN particle has a strong resonance at 535 nm and the resonance peak is near the excitation wavelength. The TiN particles can generate plasmon resonance and localized strong electric fields when irradiated by the pump laser (532 nm). The plasmon resonance can enhance the emission of the CQD and the disordered TiN particles supply strong scattering. Due to the strong random scattering, the random lasing emerges in the C/D/T composite solution. The strong electric field is also localized near TiN nanoparticles at the wavelength of 680 nm in Fig. 4(d), which indicates that when the C/D/T composite radiates photons, the TiN particles can also generate the plasmon resonance to supply a positive feedback for the generation of random lasing. In a

word, the plasmon resonance and scattering between TiN particles facilitate the lasing action in the C/D/T composite solution.

In addition, the lasing threshold of the C/D/T composite we prepared is as low as 356  $\mu\text{J}/\text{pulse}$ . There are only several lasing modes near the center wavelength, which means the high  $Q$  factor of the random lasing. Due to the narrow bandwidth emission of the C/D/T composite, the single strong peak rises at the center wavelength of 680 nm and the FWHM is 0.3 nm from Figs. 4(a) and 4(b). According to the equation of the  $Q$  factor in the random system,

$$Q = \lambda/\Delta\lambda,$$

where  $\lambda$  represents the emission center wavelength and  $\Delta\lambda$  is the FWHM of the lasing peak,  $Q = 2267$  can be obtained. Hence, the high-quality random laser in our work can be applied in the ultra-narrow wavelength range [14,16,21].

To demonstrate the energy transfer in CQD/DCM composite-doped TiN particles, the time-resolved PL spectra of CQD, CQD/DCM, and DCM are obtained by a time-correlated single-photon counter, and the molecular structures according to the FTIR spectra of pure DMSO solution, DCM solution, and CQD solution are compared. As shown in Fig. 5(a), the decay curve can be well fitted with a single exponential function with time constant of 0.72 ns for CQD, 1.11 ns for CQD/DCM, and 1.70 ns for DCM, respectively. The PL lifetime of the CQD/DCM composite exhibits the

energy transfer in CQDs and DCM nanowires [43]. The PL of the CQD/DCM composite structure has a longer lifetime compared to that of pure CQD. The reason is that part of the energy of DCM is transferred to the CQD by non-radiative transition in the composite structure, allowing more electrons in the CQD to transfer to excited states and producing more photoluminescence. Thus, the PL lifetime is extended. The PL lifetime of the CQD/DCM composite structure is shorter than that of the pure DCM, which also suggests that part of the DCM energy in the composite structure is consumed in the form of faster non-radiation transition [21]. Here, we infer that the energy is transferred to the CQD. The PL lifetime decay curves of the three elements indicate that the non-radiation transition occurs in the CQD/DCM composite structure. Therefore, the FRET process between the CQD and DCM in the composite occurs, which is consistent with the published results by Kang's group [15].

Figure 5(b) shows the FTIR spectra of the chemical structures and functional groups in pure DMSO solution, DCM solution, and CQD solution, respectively. The black curve is the FTIR spectrum of DMSO, and the main characteristic peaks have been marked with arrows in the figure. The peak at 1033  $\text{cm}^{-1}$  represents the S=O bond vibration stretching modes, and the peak at 1309  $\text{cm}^{-1}$  indicates the symmetric vibrations of  $-\text{CH}_3$  groups. The peaks at 1404 and 1434  $\text{cm}^{-1}$  indicate asymmetrical vibrations of  $-\text{CH}_3$  groups. The peaks at 2910 and 3001  $\text{cm}^{-1}$  are characteristic of the  $-\text{CH}_3$  bond

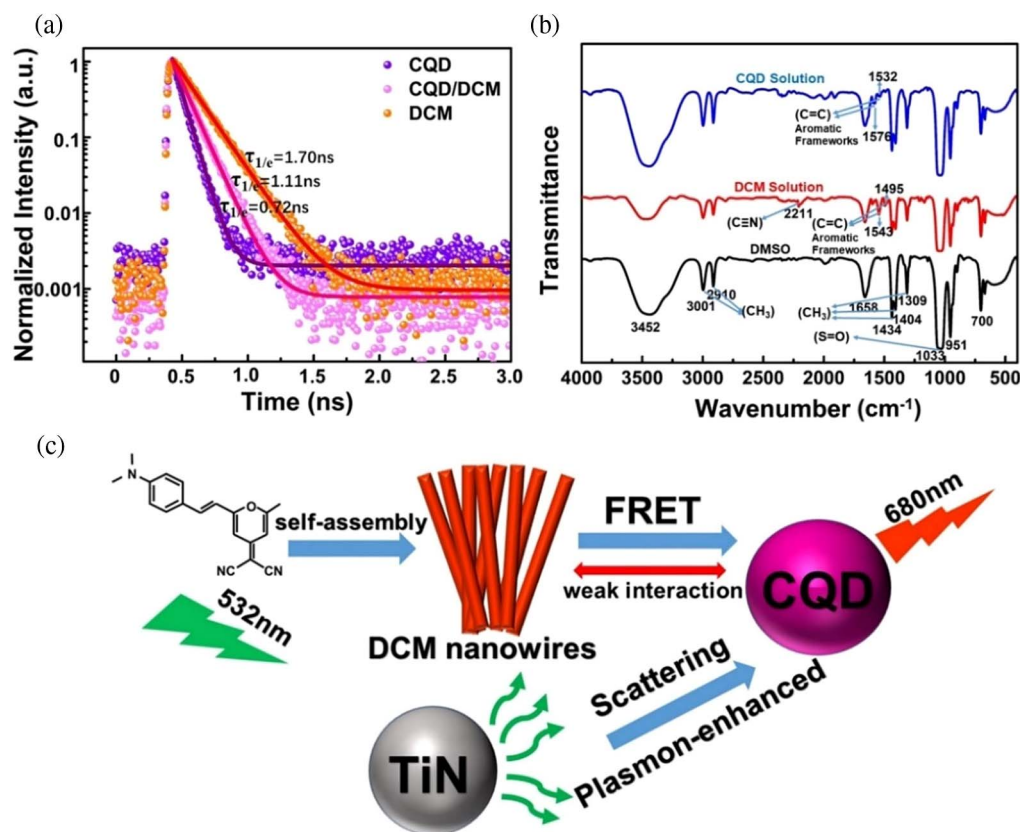


**Fig. 5.** (a) The time-resolved PL spectra of CQD, CQD/DCM, and DCM. (b) The FTIR spectra of pure DMSO solution, DCM solution (the solvent is DMSO), and CQD solution (the solvent is DMSO). (c) Schematic representation of the lasing process in the system of CQD/DCM nanowires composite-doped TiN particles.

vibrations in the region of 4000–2500  $\text{cm}^{-1}$  [44]. The red curve is the spectrum of the DCM solution. Compared with the black curve of DMSO, in addition to the same characteristic peaks of DMSO, the peak at 2211  $\text{cm}^{-1}$  indicates the  $\text{C}\equiv\text{N}$  bond vibration stretching modes and the peaks at 1495 and 1543  $\text{cm}^{-1}$  indicate the  $\text{C}=\text{C}$  bond vibration stretching modes (aromatic frameworks), which can be concluded as a benzene ring structure in DCM molecules. The blue curve is the spectrum of the CQD solution and the peaks at 1532 and 1576  $\text{cm}^{-1}$  are characteristics of the  $\text{C}=\text{C}$  bond vibration. Considering that most carbon quantum dots are aromatic framework structures, the  $\text{C}=\text{C}$  bond also indicates benzene ring structures in the CQD sample solution. By comparing DCM and CQD FTIR spectra with the DMSO spectrum, we can figure out the chemical bonds in the DCM and CQD. The presence of the benzene ring structure contributes to the formation of conjugated  $\pi$  bonds between DCM molecules in the solution, and the van der Waals interaction enables DCM molecules to self-assemble to nanowire structures at a high concentration of 0.7%. Since the CQD also contains a benzene ring structure, the CQD is more likely to bind to the DCM nanowires by weak interaction in the CQD/DCM composite solution, thus satisfying the distance condition for FRET [44].

Figure 5(c) gives a schematic diagram of lasing processes in the C/D/T composite. The whole lasing process includes the FRET between DCM nanowires and CQDs, the enhanced localized field generated by the plasmon resonance of TiN particles, and the random scattering of the TiN particles. The key point of the lasing process is the FRET. The FRET process requires the following three conditions: (1) both the donor and the recipient are luminescent materials, (2) the emission spectrum of the donor overlaps with the absorption spectrum of the recipient, and (3) the donor and recipient are spatially close enough with proper interactions. In the material system we prepared, the DCM dye molecules form the irregular nanowire structures by self-assembly and the CQDs in the solution are  $\text{sp}^2$  hybridized with a hexagon molecular structure [39,45,46]. Due to the van der Waals interaction between the CQD and DCM, the CQDs are attached on the surface of the DCM nanowires. The emission spectrum of DCM dye overlaps with the absorption spectrum of the CQD. Hence, the CQD/DCM composite satisfies the conditions for FRET. In addition, as a kind of metal nitride particle, TiN particles enhance the emission of the CQD/DCM composite due to the plasmon resonance and scattering effect of particles within the emission spectral range of the CQD/DCM composite, which results in the lasing action in the CQD/DCM composite eventually.

Therefore, when the pump light (532 nm) irradiates the CQD/DCM composite, the irregular DCM nanowire structures generate many random modes in the PL spectra. Then the energy is transferred to the CQDs from the DCM dyes via the FRET process. When TiN particles are doped in the mixture, the fluorescence of the composite is enhanced by the plasmon resonance and random scattering of TiN particles. Eventually, the ultra-narrow single-mode lasing actions emerge in the CQD/DCM/TiN composite and the lasing peaks are observed at 680 nm.

## 4. CONCLUSION

In summary, we demonstrate low-threshold, narrowband, and stable random lasing in the mixture system of CQD/DCM nanowire composite doped with TiN nanoparticles. The DCM nanowires were prepared by a self-assembled process. We found the FRET-induced lasing peaks in the CQD/DCM composite. The significant single-mode lasing emerges in the C/D/T composite due to the enhancement of plasmon resonance and scattering by TiN particles [18,42], which indicates a novel and high-Q random laser. Hence, the random lasing in the presented CQD mixture provides an avenue to realize next-generation high-brightness, high-monochromaticity random laser devices.

**Funding.** Graduate Interdisciplinary Innovation Project of Yangtze Delta Region Academy of Beijing Institute of Technology (Jiaxing) (GIIP2021-019); National Natural Science Foundation of China (62005051); National Key Research and Development Program of China (2018YFC2001100).

**Acknowledgment.** The authors would like to thank Suzhou Xingshuo Nanotech Company for the supplies of carbon dots primary material and SEM inset of carbon dots.

**Disclosures.** The authors declare no conflicts of interest.

**Data Availability.** Data underlying the results presented in this paper are not publicly available at this time but may be obtained from the authors upon reasonable request.

## REFERENCES

1. D. Wiersma, "The smallest random laser," *Nature* **406**, 133–135 (2000).
2. Z. Yang, W. Zhang, R. Ma, X. Dong, S. L. Hansen, X. Li, and Y. Rao, "Nanoparticle mediated microcavity random laser," *Photonics Res.* **5**, 557–560 (2017).
3. Y.-P. Peng, W. Lu, P. Ren, Y. Ni, Y. Wang, L. Zhang, Y.-J. Zeng, W. Zhang, and S. Ruan, "Integration of nanoscale light emitters: an efficient ultraviolet and blue random lasing from  $\text{NaYF}_4:\text{Yb/Tm}$  hexagonal nanocrystals," *Photonics Res.* **6**, 943–947 (2018).
4. S. Gao, J. Wang, W. Li, X. Yu, X. Zhang, X. Song, A. Ijijn, I. Drevensek-Olenik, R. A. Rupp, and J. Xu, "Low threshold random lasing in dye-doped and strongly disordered chiral liquid crystals," *Photonics Res.* **8**, 642–647 (2020).
5. S. Yuan, D. Chen, X. Li, J. Zhong, and X. Xu, "In situ crystallization synthesis of  $\text{CsPbBr}_3$  perovskite quantum dot-embedded glasses with improved stability for solid-state lighting and random upconverted lasing," *ACS Appl. Mater. Interfaces* **10**, 18918–18926 (2018).
6. G. Sarantoglou, M. Skontrani, A. Bogris, and C. Mesaritakis, "Experimental study of neuromorphic node based on a multiwaveband emitting two-section quantum dot laser," *Photonics Res.* **9**, B87–B95 (2021).
7. A. Y. Liu, S. Srinivasan, J. Norman, A. C. Gossard, and J. E. Bowers, "Quantum dot lasers for silicon photonics [Invited]," *Photonics Res.* **3**, B1–B9 (2015).
8. L. Yang, T. Wang, Q. Min, C. Pi, F. Li, X. Yang, K. Li, D. Zhou, J. Qiu, X. Yu, and X. Xu, "Ultrahigh photo-stable all-inorganic perovskite nanocrystals and their robust random lasing," *Nano. Adv.* **2**, 888–895 (2020).
9. D. S. Wiersma, "The physics and applications of random lasers," *Nat. Phys.* **4**, 359–367 (2008).

10. H. Cao, "Lasing in random media," *Waves Random Media* **13**, R1–R39 (2003).
11. M. Cao, Y. Zhang, X. Song, Y. Che, H. Zhang, H. Dai, G. Zhang, and J. Yao, "Random lasing in a colloidal quantum dot-doped disordered polymer," *Opt. Express* **24**, 9325–9331 (2016).
12. F. Luan, B. Gu, A. S. L. Gomes, K.-T. Yong, S. Wen, and P. N. Prasad, "Lasing in nanocomposite random media," *Nano Today* **10**, 168–192 (2015).
13. W. Zhang, Y. Ni, X. Xu, W. Lu, P. Ren, P. Yan, C. K. Siu, S. Ruan, and S. F. Yu, "Realization of multiphoton lasing from carbon nanodot microcavities," *Nanoscale* **9**, 5957–5963 (2017).
14. F. Yuan, Z. Xi, X. Shi, Y. Li, X. Li, Z. Wang, L. Fan, and S. Yang, "Ultraportable and low-threshold random lasing from narrow-bandwidth-emission triangular carbon quantum dots," *Adv. Opt. Mater.* **7**, 1801202 (2019).
15. A. Yadav, L. Bai, Y. Yang, J. Liu, A. Kaushik, G. J. Cheng, L. Jiang, L. Chi, and Z. Kang, "Lasing behavior of surface functionalized carbon quantum dot/RhB composites," *Nanoscale* **9**, 5049–5054 (2017).
16. Y. Ni, H. Wan, W. Liang, S. Zhang, X. Xu, L. Li, Y. Shao, S. Ruan, and W. Zhang, "Random lasing carbon dot fibers for multilevel anti-counterfeiting," *Nanoscale* **13**, 16872–16878 (2021).
17. Y. Ni, X. Li, W. Liang, S. Zhang, X. Xu, Z. Li, L. Li, Y. Shao, S. Ruan, and W. Zhang, "Transformation of random lasing to Fabry–Perot lasing: observation of high temperature lasing from carbon dots," *Nanoscale* **13**, 7566–7573 (2021).
18. W.-C. Liao, Y.-M. Liao, C.-T. Su, P. Perumal, S.-Y. Lin, W.-J. Lin, C.-H. Chang, H.-I. Lin, G. Haider, C.-Y. Chang, S.-W. Chang, C.-Y. Tsai, T.-C. Lu, T.-Y. Lin, and Y.-F. Chen, "Plasmonic carbon-dot-decorated nanostructured semiconductors for efficient and tunable random laser action," *ACS Appl. Nano Mater.* **1**, 152–159 (2018).
19. C. Gollner, J. Ziegler, L. Protesescu, D. N. Dirin, R. T. Lechner, G. Fritz-Popovschi, M. Sytnyk, S. Yakunin, S. Rotter, A. A. Yousefi Amin, C. Vidal, C. Hrelescu, T. A. Klar, M. V. Kovalenko, and W. Heiss, "Random lasing with systematic threshold behavior in films of CdSe/CdS core/thick-shell colloidal quantum dots," *ACS Nano* **9**, 9792–9801 (2015).
20. F. Di Stasio, A. Polovitsyn, I. Angeloni, I. Moreels, and R. Krahné, "Broadband amplified spontaneous emission and random lasing from wurtzite CdSe/CdS "giant-shell" nanocrystals," *ACS Photonics* **3**, 2083–2088 (2016).
21. Y.-J. Lee, T.-W. Yeh, C. Zou, Z.-P. Yang, J.-W. Chen, P.-L. Hsu, J.-L. Shen, C.-C. Chang, J.-K. Sheu, and L. Y. Lin, "Graphene quantum dot vertical cavity surface-emitting lasers," *ACS Photonics* **6**, 2894–2901 (2019).
22. O. N. Karpov, G. N. Bondarenko, A. S. Merekalov, G. A. Shandryuk, O. M. Zhigalina, D. N. Khmelenin, E. A. Skryleva, L. A. Golovan, and R. V. Talroze, "Formation of the inorganic and organic shells on the surface of CdSe quantum dots," *ACS Appl. Mater. Interfaces* **13**, 36190–36200 (2021).
23. H. Zhu, W. Zhang, and S. F. Yu, "Realization of lasing emission from graphene quantum dots using titanium dioxide nanoparticles as light scatterers," *Nanoscale* **5**, 1797–1802 (2013).
24. W. F. Zhang, L. M. Jin, S. F. Yu, H. Zhu, S. S. Pan, Y. H. Zhao, and H. Y. Yang, "Wide-bandwidth lasing from C-dot/epoxy nanocomposite Fabry–Perot cavities with ultralow threshold," *J. Mater. Chem. C* **2**, 1525–1531 (2014).
25. Y. Li, K. Xie, X. Zhang, Z. Hu, J. Ma, X. Chen, J. Zhang, Z. Liu, and D. Chen, "Coherent random lasing realized in polymer vesicles," *Photon. Sens.* **10**, 254–264 (2020).
26. G. Weng, J. Yan, S. Chen, C. Zhao, H. Zhang, J. Tian, Y. Liu, X. Hu, J. Tao, S. Chen, Z. Zhu, H. Akiyama, and J. Chu, "Superior single-mode lasing in a self-assembly CsPbX<sub>3</sub> microcavity over an ultrawide pumping wavelength range," *Photonics Res.* **9**, 54–65 (2021).
27. S. C. Singh and R. Gopal, "Drop shaped zinc oxide quantum dots and their self-assembly into dendritic nanostructures: liquid assisted pulsed laser ablation and characterizations," *Appl. Surf. Sci.* **258**, 2211–2218 (2012).
28. S. Kedia, R. Vijaya, A. K. Ray, and S. Sinha, "Spectral narrowing and lasing threshold in self-assembled active photonic crystal," *Opt. Commun.* **284**, 2056–2060 (2011).
29. R. Yang, Z. Hu, Y. Li, J. Xia, J. Ma, and J. Yang, "Spray coated perylenebisimide/polymer film with controllable molecular aggregation state and emission properties," *RSC Adv.* **10**, 2437–2447 (2020).
30. P. Rafieipour, A. G. Ardakani, and F. Daneshmand, "Resonant random laser emission from graphene quantum dots doped dye solution," *Laser Phys.* **30**, 115003 (2020).
31. R. Xiong, S. Yu, M. J. Smith, J. Zhou, M. Krecker, L. Zhang, D. Nepal, T. J. Bunning, and V. V. Tsukruk, "Self-assembly of emissive nanocellulose/quantum dot nanostructures for chiral fluorescent materials," *ACS Nano* **13**, 9074–9081 (2019).
32. C. Wei, S.-Y. Liu, C.-L. Zou, Y. Liu, J. Yao, and Y. S. Zhao, "Controlled self-assembly of organic composite microdisks for efficient output coupling of whispering-gallery-mode lasers," *J. Am. Chem. Soc.* **137**, 62–65 (2015).
33. Y. Wang, H. Li, L. Zhao, Y. Liu, S. Liu, and J. Yang, "Tunable whispering gallery modes lasing in dye-doped cholesteric liquid crystal microdroplets," *Appl. Phys. Lett.* **109**, 231906 (2016).
34. D. Venkatakishnarao and R. Chandrasekar, "Engineering the self-assembly of DCM dyes into whispering-gallery-mode  $\mu$ -hemispheres and Fabry–Pérot-type  $\mu$ -rods for visible–NIR (600–875 nm) range optical microcavities," *Adv. Opt. Mater.* **4**, 112–119 (2016).
35. K. Sunita, V. Ramarao, K. R. Alok, and S. Sucharita, "Laser emission from self-assembled active photonic crystal matrix," *J. Nanophotonics* **4**, 049506 (2010).
36. L. Cerdán, A. Costela, E. Enciso, and I. García-Moreno, "Random lasing in self-assembled dye-doped latex nanoparticles: packing density effects," *Adv. Funct. Mater.* **23**, 3916–3924 (2013).
37. L.-J. Chen, J.-H. Dai, J.-D. Lin, T.-S. Mo, H.-P. Lin, H.-C. Yeh, Y.-C. Chuang, S.-A. Jiang, and C.-R. Lee, "Wavelength-Tunable and highly stable perovskite-quantum-dot-doped lasers with liquid crystal lasing cavities," *ACS Appl. Mater. Interfaces* **10**, 33307–33315 (2018).
38. F. Yuan, L. Ding, Y. Li, X. Li, L. Fan, S. Zhou, D. Fang, and S. Yang, "Multicolor fluorescent graphene quantum dots colorimetrically responsive to all-pH and a wide temperature range," *Nanoscale* **7**, 11727–11733 (2015).
39. H. Liu, F. Wang, Y. Wang, J. Mei, and D. Zhao, "Whispering gallery mode laser from carbon dot–NaCl hybrid crystals," *ACS Appl. Mater. Interfaces* **9**, 18248–18253 (2017).
40. S.-H. Kim, S.-H. Kim, W. C. Jeong, and S.-M. Yang, "Low-threshold lasing in 3D dye-doped photonic crystals derived from colloidal self-assemblies," *Chem. Mater.* **21**, 4993–4999 (2009).
41. S. Zhang, Y. Li, P. Hu, Z. Tian, Q. Li, A. Li, Y. Zhang, and F. Yun, "Realization of directional single-mode lasing by a GaN-based warped microring," *Photonics Res.* **9**, 432–438 (2021).
42. K. Cyprych, D. Chateau, A. Désert, S. Parola, and J. Mysliwiec, "Plasmonic nanoparticles driven enhanced light amplification in a local 2D and 3D self-assembly," *Nanomaterials* **8**, 1051 (2018).
43. L. Huang, D. Zhang, C. Ge, M. He, Z. Zeng, Y. Wang, S. Liu, X. Wang, and A. Pan, "Enhancing circular polarization of photoluminescence of two-dimensional Ruddlesden–Popper perovskites by constructing van der Waals heterostructures," *Appl. Phys. Lett.* **119**, 151101 (2021).
44. D. Lai, T. Liu, X. Gu, Y. Chen, J. Niu, L. Yi, and W. Chen, "Suspension synthesis of surfactant-free cuprous oxide quantum dots," *J. Nanomater.* **2015**, 825021 (2015).
45. M. Zavelani-Rossi, M. G. Lupo, R. Krahné, L. Manna, and G. Lanzani, "Lasing in self-assembled microcavities of CdSe/CdS core/shell colloidal quantum rods," *Nanoscale* **2**, 931–935 (2010).
46. E. Avellanal-Zaballa, J. Bañuelos, H. Manzano, J. L. Chiara, L. Cerdán, and I. García-Moreno, "Taming the photonic behavior of laser dyes through specific and dynamic self-assembly onto cellulose nanocrystals," *Adv. Photonics Res.* **2**, 2000107 (2021).